Journal of Petroleum Research and Studies

Open Access
No. 40, September 2023, pp. 19-40

P- ISSN: 2220-5381
E- ISSN: 2710-1096

DOI: http://doi.org/10.52716/jprs.v13i3.729

Petrography and Geochemistry of Zubair Shale Formation in Rumaila Oilfield, Southern Iraq: Implications for Provenance and Tectonic Setting

Rana Abbas Ali

Department of Geology, College of Science, University of Baghdad, Iraq

*Corresponding author E-mail: rana.ali@sc.uobaghdad.edu.iq

Received 26/12/2022, Revised 15/03/2023, Accepted 22/03/2023, Published 10/09/2023

Abstract

A detailed sequential analysis which included thin section petrography, X-ray diffraction, and X-ray fluorescence was applied to investigate the mineral, chemical classifications, provenance, paleo-weathering, paleoclimate, and maturity features of such Zubair oil shale in the Rumaila oilfield in southern Iraq. In core samples and thin sections, the analyzed shales are primarily silty, flaky to subflaky, micaceous, calcareous, well-sorted, poorly cemented, and weakly to moderately compacted silt-grade sandy mudstone. According to XRD analysis, the main mineral is quartz, which is followed by kaolinite, while calcite and dolomite are less common and Illite, Illite/smectite, and pyrite are rarely abundant. Petrographic analysis of the Zubair shales revealed four lithofacies: silty clayey laminated mudstone lithofacies, mica-rich mudstone lithofacies, clay-rich siliceous mudstone lithofacies, and clay-bearing calcareous mudstone lithofacies. Major and trace element concentrations reveal that the oil shales have been formed from felsic rocks such as granodiorite, tonalite, and granite. A passive margin setting was revealed by the tectonic discrimination diagram. Weathering index values like the (CIA) chemical index of alteration, the (PIA) plagioclase index of alteration, and the (CIW) chemical index of weathering imply extensive chemical weathering in the source area. Zubair shales' K2O/Na2O ratio and (ICV) index of compositional variation are uniform with their high maturity. The compositions of mineral and trace elemental ratios, as well as the climatic index "C," indicate a warm to humid subtropical climate with deposition in a shallow oxic and dysoxic environment.

Keywords: Paleoclimate, Paleo-weathering, Provenance, Tectonic setting, Zubair shales.

1. Introduction:

Lower Cretaceous deposits, particularly in Southern Iraq, are extremely valuable due to significant hydrocarbon accumulations but also reservoirs (Fig. 1A). The Zubair Formation is part of the Late Berriasian-Albian cycle formations, due to its excellent reservoir properties, it

Open Access
No. 40, September 2023, pp. 19-40
P- ISSN: 2220-5381
E- ISSN: 2710-1096

can be considered an important reservoir in southern Iraq and neighboring countries [1]. It is interesting to note that the shale constituents are the source lithology within the formation, even though they contain some rare elements and pyrite, which demonstrate a depositional environment that is reductive and acidic. Rocks known as source rocks have an abundance of organic material that, when heated and compressed over time, can yield hydrocarbons. Shales and limestones are the most common source rocks (i.e., sedimentary rocks). This evidence backs up the hypothesis that the source rock created in the Zubair Formation [2]. Such a formation is comprised of multiple depositional cycles. So every cycle represents the forming of a deltaic lobe (construction phase), then by a prolonged break after which the delta margin has been subjected to tidal action and wave (destruction phase). Finally, the cycle was completed by the formation of a marine transgressive shale. However, when growth of a deltaic lobe has been renewed above a shale base, a new cycle starts [3]. The Zubair Formation is dominated by sequences of siliciclastic lithostratigraphic, with lim. constrained towards the Formation's upper portion, which represents a transgressive phase. The shale packs thin out toward the west of the research, whereas the coarse clastic packs thin out toward the east [4]. The Zubair Formation's upper contact was defined by the presence of shale following the Shuaiba Carbonate Formation, while the lower contact was defined by the presence of the Ratawi Limestone Formation (Fig. 1B). [5] studied trialing and assessment of shale stabilization for Zubair Shale Formation. [6] investigated the geochemistry of the Zubair Formation (upper shale member) in both northern and southern Rumaila oilfield also compared between the major and trace elements in both fields.

Based on mineralogical and geochemical features, the study aims to examine the mineral, chemical classifications, paleo-weathering, provenience, paleoclimate and maturity features of the upper, middle and lower oil shale members in the research areas. This makes it possible to research oil shale's composition, quality parameters, and formation process. Additionally, since 1953 in Rumaila Oilfields, the Zubair oil shale's industrial quality has been evaluated. It's also necessary to re-assess the efficiency of Zubair oil shale, to provide new parameters for the future assessment of oil shale in the Rumaila Oilfield in the context of improving current experimental technology.

2. Geological setting

The area of the current study is located in the north and south Rumaila oilfield, which is part of the Mesopotamian zone of the stable shelf division (Figure 1). Zubair, Euphrates, and Tigris

Open Access
No. 40, September 2023, pp. 19-40
P- ISSN: 2220-5381
E- ISSN: 2710-1096

subzones comprise the Mesopotamian Zone. This research's proposal is Zubair subzones, and the area is defined by latitude 30°00'-30°45'N and longitude 47°00'-47°30'E. The Zubair Subzone has been identified by numerous enlarged folds extending from the north to the northwest to the southeast, representing Basra province's vast oilfields [7]. These folds, which were eventually confined in the Late Cretaceous, were defined by narrow and linear anticlines with few clues of faulted basement stone [4], Rumaila North (R) and Rumaila South (Ru) are the oil fields in this subzone of interest. The formation in Zubair Subzone is classified: Upper shale member, Upper sandstone member, Middle shale member, Lower sandstone member, and Lower shale member.

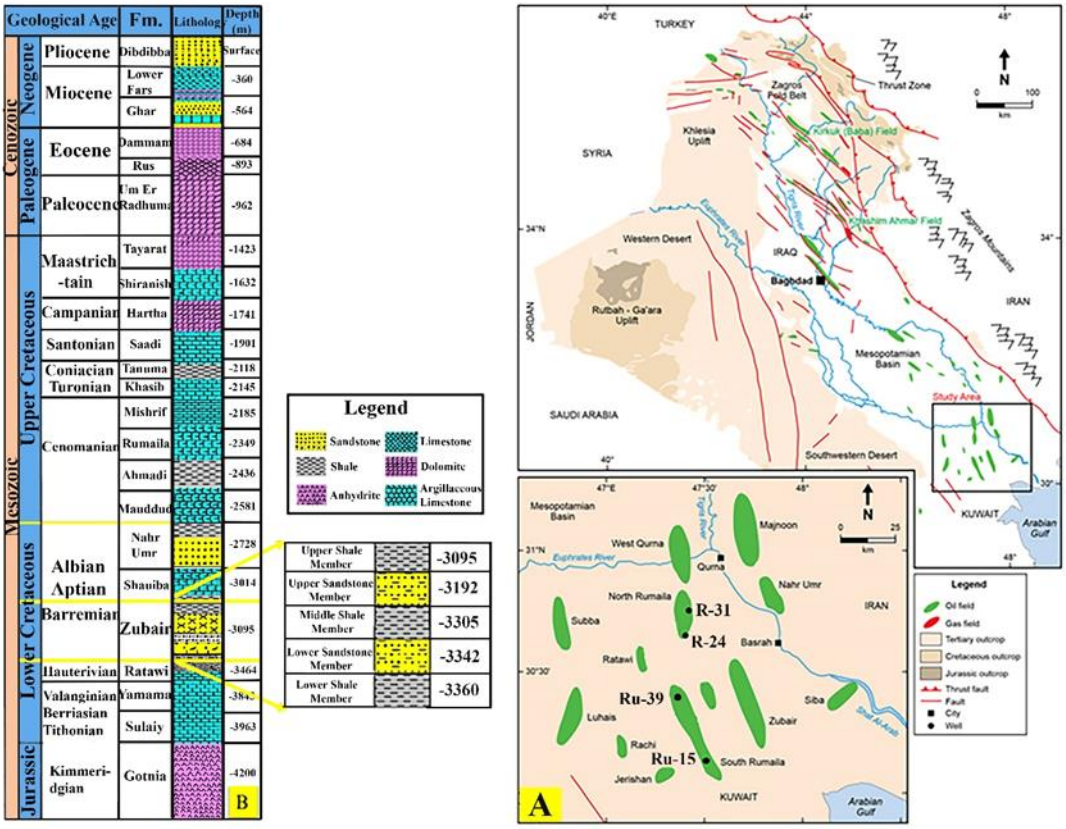

Fig. (1): (A) Location map of the investigated wells and oil fields, (B) stratigraphic column in southern Iraq for the study area [8].

3. Materials and Methods

Samples of Zubair Formation were collected from four boreholes drilled by the South Oil Company in the north and south Rumaila Oilfield in the Zubair Subzone, Southern Iraq. These wells are R-31 (3030-3350 m sampling depth), R-24 (3160-3360 m sampling depth), Ru-15 (3100-3357 m sampling depth), and Ru-39 (3095-3350 m sampling depth) (Table 1). To examine

Open Access
No. 40, September 2023, pp. 19-40
P- ISSN: 2220-5381
E- ISSN: 2710-1096

the main components and determine the primary lithofacies, 35 thin sections of Zubair shales were prepared. Powder XRD mineralogical analysis was performed on 50 grams of the sample.

The objective is to identify the mineralogy and semi-quantitatively analyze it using the ICDD database and the High Score Plus software. The powdered specimens for geochemical analyses have been heated at 105ºC in the presence of oxygen to remove any remaining volatile components and oxidized Fe. At 1000ºC, the loss on ignition (L.O.I.) of samples was determined. X-ray fluorescence (XRF) was used to determine the concentrations of major and trace elements.

Table (1) The wells and samples number of Zubair shales.

Well No.	Sample No.	Formation	Depth (m)	Oilfield	Sample type
R-31	23	Zubair	3030-3350	North Rumaila	cores
R-24	25	Zubair	3160-3360	North Rumaila	cores
Ru-15	27	Zubair	3100-3357	South Rumaila	cores
Ru-39	24	Zubair	3095- 3350	South Rumaila	cutting

4. Results and Discussions

4.1 Mineralogy

The mineral composition of five Zubair shale samples was examined using XRD experiments, which shows with petrographical study that the average quartz content (monocrystalline) in samples is 41.54 - 47.23 % (Fig.2). Quartz is a common auxiliary mineral connected with siliceous eruptions such as plutonic granite (Fig.3 A, E & F). Participating in all stages of metamorphism and possessing an elevated resistance to chemical weathering. This mineral is abundant in sedimentary rocks, along with oil shales [9]. The shale samples were rich in pore-filling detrital clays, (41.14 - 45.53 %), which including kaolinite, illite, illite/smectite and chlorite.

The alteration of feldspar and muscovite produces kaolinite. There are two types of kaolin deposits: primary and secondary. Secondary kaolin is sedimentary in origin, while primary results from residual weathering or hydrothermal alteration. Kaolinite spreads in river and lake sediments where leaching processes predominate, but it quickly turns into illite in marine environments due to its low stability. Because kaolinite grains are relatively coarse, the fluctuation process is faster, and it is therefore found in deltaic areas [10]. Illite could be of the

Open Access
No. 40, September 2023, pp. 19-40
P- ISSN: 2220-5381
E- ISSN: 2710-1096

clastic origin or the result of weathering of mica-rich igneous or metamorphic rocks. With the availability of K+, illite also forms from kaolinite in diagenesis after its transfer to the marine environment, or by increasing the depth of burial, the montmorillonite is completely transformed into illite, explaining the absence of montmorillonite in the ancient sediments [11]. Illite/Smectite is formed by the partial filtration of K+ or Mg(OH)2 between layers of illite or chlorite, followed by partial adsorption by layers of montmorillonite or vermiculite. This effect usually occurs during weathering or in the sedimentation basin, but it can also be hydrothermal in nature. Chlorites are established when physical and chemical changes occur in mafic minerals. Chlorites, which are common in low-temperature hydrothermal alteration and low-grade metamorphism, are not among the most reactive minerals to introduce into a sedimentary system. Chlorite is a prevalent detrital mineral throughout sedimentary systems since it weathers and changes slowly in the hinterlands, soils, also during transport [11].

Calcite and dolomite have low percentages in the samples, (4.74-9.42%), and (0-2.69%), respectively, dolomite is only present in a few of them (Figure 3 C, D & E). This indicates that the Zubair Formation's sedimentation environment is shallow, with a decrease in carbonate minerals and an increase in clastic minerals. Pyrite has a percentage of 2.0- 5.24%, is abundant in both ancient and recent sedimentary rocks and is the most stable iron sulfide mineral in anoxic environments at low temperatures. Framboidal pyrites have been made up of clusters of subspheroidal to spheroidal pyrite microcrystals with a raspberry-like appearance (Figure 4 A & B). Pyrite framboids have such a unique framework composed of invariable pyrite microcrystals (euhedral-shaped), which is not even interrupted by overburden pressure. Euhedral pyrite, on the other hand, is made up of a single pyrite crystal or a grouping of pyrite crystals of varying sizes (Figure 3 A). The mineral composition of Zubair shales was also plotted using a ternary graph [12], where the total contents of (QFM) quartz, feldspar, and mica, (Carbonates) calcite and dolomite, and (Clays) kaolinite, illite, illite/smectite, and chlorite all are equivalent to 100%. The findings (Fig. 5a) show that the Zubair shale in the study region is relatively rich in quartz & clay minerals but low in carbonates, implying that it is a Silica-rich argillaceous mudstone. This mineral composition is ideal for hydraulic fracturing due to the presence of a high concentration of brittle minerals. The minor differences in shale composition between wells are depicted in Figure (5b).

Open Access
No. 40, September 2023, pp. 19-40
P- ISSN: 2220-5381
E- ISSN: 2710-1096

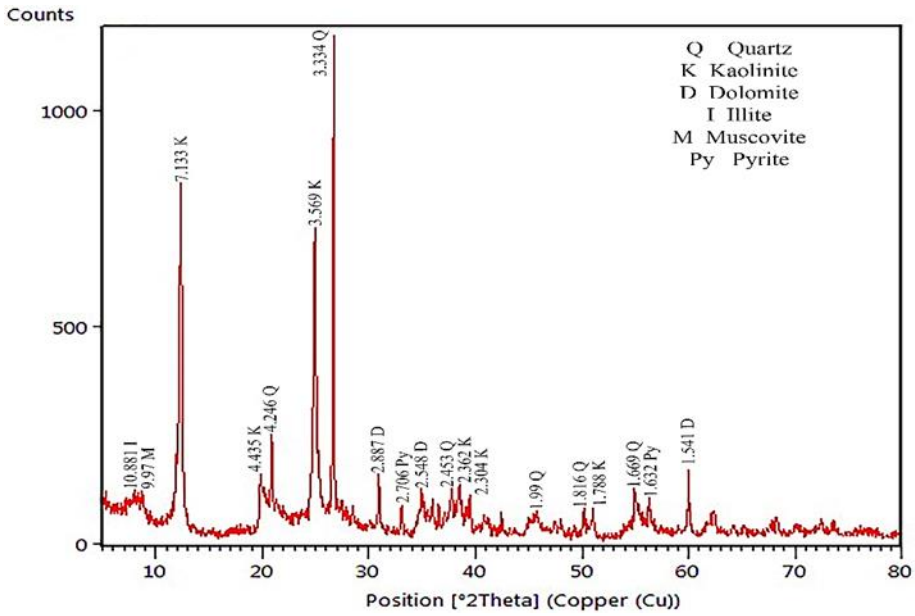

Fig. (2): Annotated XRD diffractograms of geologic source samples. Peaks are highlighted in pink, and labels above the peaks indicate d-spacing in Aº. For a Cu radiation source with a K-alpha wavelength of 1.540, the X-axis is marked by degrees 2-theta.

4.2 Petrography

Throughout the sequence, irregular laminae, lenses, and mottles of sandstones and siltstones in shale ground mass can be found. The mineralogy and textures of Zubair shale samples were studied using petrographic analysis of thin sections. The shale samples examined range in color from gray to black, and highly bituminous shales also are prevalent. The Zubair shale does have a laminated structure composed of well-sorted, badly cemented, loosely to moderately compacted, silt-grade sandy mudstone, white grains (calcite mineral), heavy minerals, black assemblies (residual hydrocarbons or pyrite), kaolinite booklets, illite, and chlorite. There is no visual macroporosity and only a little fracture (mainly 10-20 µm wide black lines) that run primarily along the bedding plane. The petrographic analysis identifies four lithofacies as follows:

1- Silty-clayey laminated mudstone lithofacies: it displays lenticular to wavy laminations of silt-sized grains also with clay minerals in size much smaller than 0.05mm (Figure 3B). The silt-size grains mostly are sub-angular to angular quartz grains, with a few pyrite and mica grains thrown in for good measure (Figure 3A). The laminations are clearly defined by the conversely of dark and light color as well as fine and coarse grain sizes. Organic particles are more abundant in clay laminae than in silt laminae. It is mostly found in the Zubair Formation's middle shale member.

Open Access
No. 40, September 2023, pp. 19-40
P- ISSN: 2220-5381
E- ISSN: 2710-1096

2- Mica-rich mudstone lithofacies: a strong compaction past has occurred in the merging of mica and clay particles (primarily muscovite) around the silica detrital particles, with organic particles defining the boundaries of these merging (Figure 3C, D). It mostly occurs in the lower shale member of the Zubair Formation.
3- Clay-rich siliceous mudstone lithofacies: It's mostly brown and black, with light laminations of clay particles and silt-sized quartz grains. A few mica flakes and organic particles have been scattered, but there are no carbonate minerals to be found (Figure 3E, F). It is mostly noticed in the Zubair Formation's middle shale member.
4- Clay bearing calcareous mudstone lithofacies: it's mostly brown, with some silt-sized quartz grains and light laminations of the dominant clay particles. A few pyrite and organic particles are scattered (Figure 3G, H). This lithofacies contains common fecal pellets with preferred orientation (Figure 4C, D). It is mostly found in the Zubair Formation's upper shale member.

Open Access
No. 40, September 2023, pp. 19-40
P- ISSN: 2220-5381
E- ISSN: 2710-1096

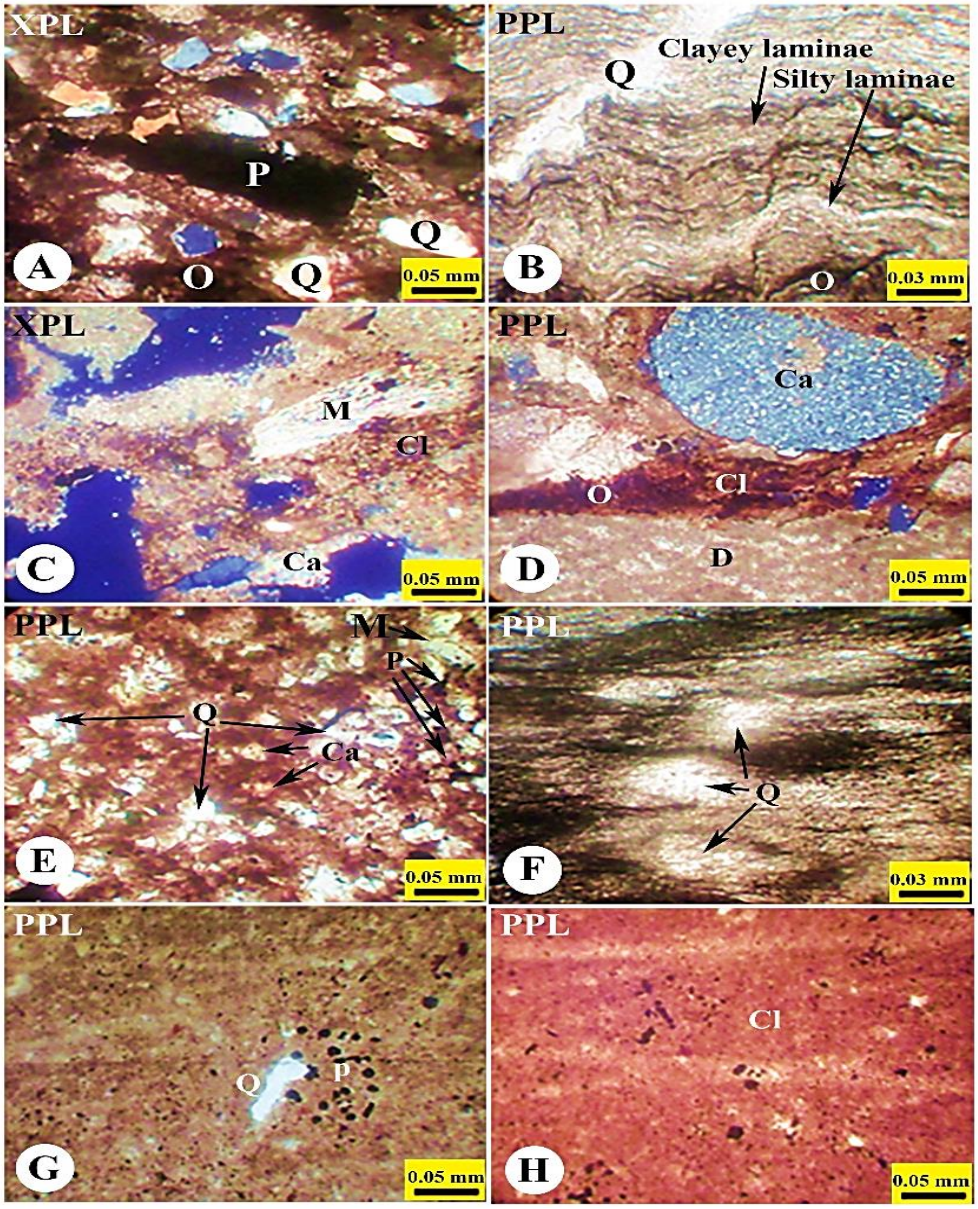

Fig. (3): Photomicrographs of shale samples of Zubair Fm. from Rumaila oilfield. (A) Silty-clayey laminated mudstone displays (Q) silt sized quartz grain dispersed in clay (ground mass), and (P) pyrite. (B) Silty-clayey laminated mudstone with (light brown) silt size, (dark brown) clay laminae and (black) organic particles (O) aligned horizontally. (C) Mica-rich lithofacies display a compacted merging of elongated mica (M), clay (Cl), and calcite (Ca), residual inter-granular pores. (D) Mica-rich lithofacies display Ca (calcite) and D (dolomite) in clay ground mass (Cl). (E) Clayey-rich lithofacies display the dispersed nature of quartz detritus (Q), mica (M), and pyrite framboid (P) in clay groundmass. (F) (G) and (H) a gentle lamination pattern.

Open Access
No. 40, September 2023, pp. 19-40
P- ISSN: 2220-5381
E- ISSN: 2710-1096

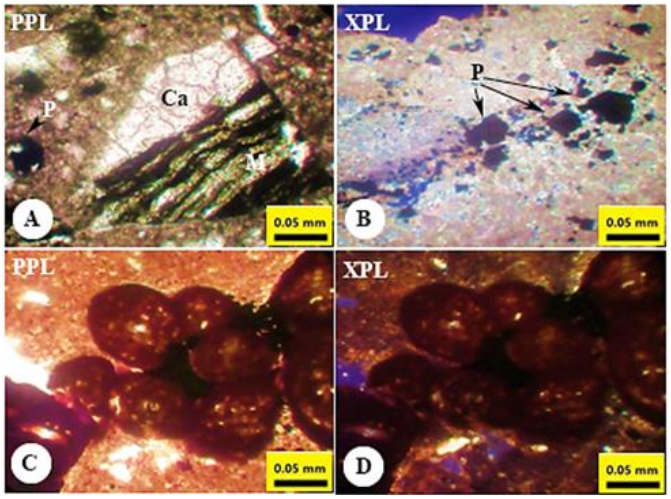

Fig. (4) Photomicrographs of shale samples of Zubair Fm. from Rumaila oilfield. (A) calcite with mica grain and framboidal pyrites. (B) Framboidal pyrites. (C) & (D) facial pellets.

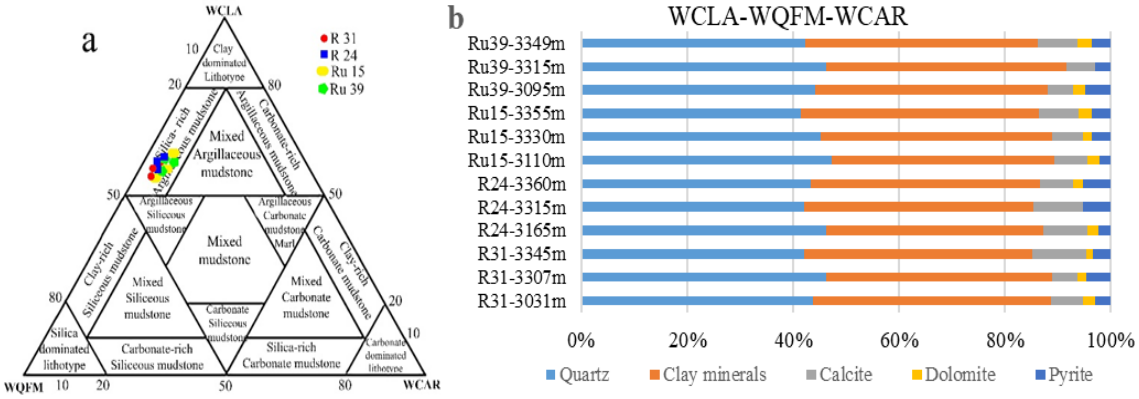

Fig. (5): (a) The lithotype classification relies on a ternary graph of the mineral composition of Zubair shale samples from the Rumaila oilfield, as modified by [12]; (b) XRD and thin-section point counting charts depicting stratigraphic variation in the composition of shale samples from the R31, R24, Ru15, and Ru39 wells.

4.3 Geochemistry (Major and Trace Elements)

Major & trace elements concentrations for Zubair shale samples (R31, R24, Ru15, Ru39; n= 12) are shown in Tables (2) and (3). Similar concentrations can be found in the oil shales from the Rumaila oilfield. The SiO_2, Al_2O_3, and Fe_2O_3 abundances differ from 52.88 to 70.33 wt. % (av.= 60.87), 12.25 to 21.91 wt. % (av.= 16.04), and 1.66 to 6.42 wt. % (av.= 3.92), respectively. The abundance of clay minerals is associated with the high content of Al_2O_3. TiO_2 content of Zubair shales ranges from 0.78 to 1.28 wt. % (ave.= 1.06). The average of alkali (Na^+, K^+), alkaline-earth (Ca^{2+}, Mg^{2+}), and SO_3 contents in the shales are 1-2 wt. %.

Open Access
No. 40, September 2023, pp. 19-40
P- ISSN: 2220-5381
E- ISSN: 2710-1096

Table (2) Shows the major elements (weight percentages) by XRF, and some elemental ratios of the Zubair shale samples.

Sample No.	R31-1	R31-2	R31-3	R24-1	R24-2	R24-3	Ru15-1	Ru15-2	Ru15-3	Ru39-1	Ru39-2	Ru39-3	Mean Σ
Depth m.	3031	3307	3345	3165	3315	3360	3110	3330	3355	3095	3315	3349	
SiO_2	59.55	54.23	60.41	53.80	64.06	52.88	66.77	67.22	61.34	55.71	64.25	70.33	60.87
Al_2O_3	18.23	15.93	14.67	15.87	15.26	14.65	13.93	12.25	19.32	21.91	16.98	13.49	16.04
Fe_2O_3	3.27	4.97	5.62	6.23	6.42	4.76	3.30	3.24	2.33	1.66	3.26	2.00	3.92
CaO	0.21	0.36	1.67	1.23	0.11	2.45	0.12	1.02	0.98	1.32	1.97	1.78	1.10
MgO	1.02	2.65	1.49	1.87	1.41	2.45	2.56	2.17	1.28	0.94	1.24	1.98	1.75
Na_2O	1.15	1.05	1.03	0.99	1.12	0.93	1.09	0.52	1.10	0.29	1.02	0.98	0.94
K_2O	2.96	3.75	2.15	2.19	2.64	2.71	1.21	1.93	2.46	1.80	2.16	1.14	2.25
TiO_2	1.02	1.12	1.00	1.12	0.99	1.24	0.95	0.78	1.28	1.27	1.09	0.88	1.06
SO_3	1.26	1.32	1.55	0.98	1.45	1.85	0.77	1.66	1.16	1.09	1.57	0.98	1.30
L.O.I	10.85	14.4	9.66	15.48	6.43	15.53	9.06	8.95	8.45	13.88	5.53	6.42	10.38
Total	99.52	99.78	99.25	99.76	99.89	99.45	99.76	99.74	99.70	99.87	99.07	99.98	99.61
K_2O/Na_2O	2.57	3.57	2.08	2.21	2.35	2.91	1.11	3.71	2.23	6.2	2.11	1.16	2.68
Al_2O_3/TiO_2	17.87	14.22	14.67	14.16	15.41	11.81	14.66	15.7	15.09	17.25	15.57	15.32	15.14
SiO_2/Al_2O_3	3.26	3.4	4.11	3.39	4.19	3.6	4.79	5.48	3.17	2.54	3.78	5.21	3.91
CIA	80.84	75.53	75.15	78.25	79.76	70.63	85.19	77.92	80.97	86.53	76.72	77.57	78.75
PIA	91.82	89.62	82.26	86.03	88.54	82.37	91.31	87.01	89.01	92.58	83.21	81.73	87.12
CIW	93.05	91.86	84.45	87.72	92.54	81.25	92	88.83	90.28	93.15	85.02	83.01	88.59
ICV	0.52	0.87	0.88	0.85	0.83	0.99	0.66	0.78	0.48	0.33	0.63	0.65	0.70

CIA (%) = $[Al_2O_3/ (Al_2O_3 + Na_2O+ K_2O+ CaO^*)] \times 100$ from [13]
PIA (%) = $[Al_2O_3-K_2O/ (Al_2O_3 + Na_2O+ K_2O+ CaO)] \times 100$ from [14]
CIW (%) = $[Al_2O_3/ (Al_2O_3 + Na_2O+CaO^*)] \times 100$ from [15]
ICV (%) = $(Fe_2O_3+ CaO+K_2O+ MgO +Na_2O+ TiO_2+MnO)/Al_2O_3$ from [16].
In which CaO* correction was used, the procedure of [17] was followed.

Table (3) shows the trace elements (ppm) by XRF, and elemental ratios of Zubair shale samples.

Sample No.	R31-1	R31-2	R31-3	R24-1	R24-2	R24-3	Ru15-1	Ru15-2	Ru15-3	Ru39-1	Ru39-2	Ru39-3	Mean Σ
Depth m.	3031	3307	3345	3165	3315	3360	3110	3330	3355	3095	3315	3349	
Mn	466	76	238	62	175	29	52	38	22	87	27	63	111.25
Sr	144.54	220.43	90.69	100.55	62.78	300.66	25.25	55.89	46.78	34.98	85.42	64.99	102.74
Ba	166.5	143.7	88.3	195.7	163.8	90.4	275	140.5	290	416	300	130	199.99
V	77.5	81	90	50	100	62	57	40	35	27	56	77	62.70
Ni	173	125	72	94	115	130	67	74	90	106	15	59	95
Cr	56	34	147	112	44	19	23	36	56	34	65	18	53.66
Zn	167	120	472	309	190	227	32	78	67	191	234	333	201.66
Cu	52	79	42	35	136	84	15	32	13	49	41	28	50.50
Zr	334	556	398	457	589	479	178	259	364	119	168	78	131.58
Rb	21	39	13	29	18	33	15	12	11	18	23	27	21.58
Co	20	29	40	38	44	18	23	27	13	67	9	17	28.75
Rb/Sr	0.14	0.17	0.14	0.28	0.28	0.11	0.59	0.21	0.23	0.51	0.26	0.41	0.21
Sr/Cu	2.77	2.79	2.15	2.87	0.46	3.57	1.68	1.74	3.59	0.71	2.08	2.32	2.03
Ni/Co	8.65	4.31	1.8	2.47	2.61	7.22	2.91	2.74	6.92	1.58	1.66	3.47	3.30
C	0.57	0.66	0.75	0.63	0.78	0.82	0.72	0.76	0.81	0.74	0.68	0.64	0.71

The shales also have a high (L.O.I) loss on ignition, that ranges from 5.53 to 15.53 wt.% (av.= 10.38 wt.%) and is due to the presence of clay minerals and organic matter. Figure (6) depicts the relationship between Al_2O_3 and major elements. The inverse relationship between SiO_2 and Al_2O_3 is a result of the fact that quartz contains the majority of the silica. The positive correlation

Open Access
No. 40, September 2023, pp. 19-40
P- ISSN: 2220-5381
E- ISSN: 2710-1096

between K_2O, Na_2O, L.O.I, Fe_2O_3, TiO_2, and SO_3 with Al_2O_3 suggests that silicates are primarily responsible for their distribution [18].

The Zubair Shale Formation appears in shale fields on the [19] diagram (Figure 7a, b). Samples schemed in a shale field could reflect the clay minerals correlation, and source rocks can be felsic to intermediate in composition.

Table (3) displays the trace element concentrations obtained from 12 oil shale specimens. Transitional trace element concentrations (for example, Mn, V, Ni, Cr, Zn, Cu, Zr, and Co) varied little in core shale. The existence of calcite and dolomite may explain the Sr concentration (25.25 to 300.66 ppm) in Zubair shale. The occurrence of large-ion lithosphere components (e.g., Sr, Ba, and Rb) in sheet silicates such as illite and illite-smectite suggests incorporation, as well as adsorbent on to the clay mineral substrates.

Figure (8) depicts the elemental constituents of the Zubair shale normalized to chondrite and (PAAS) Post Archean Australian Shale [20]. The proportion of the major and trace elements at various specimens is equivalent to that of chondrite and PAAS. Al_2O_3, Na_2O, K_2O, and TiO_2 are enriched comparative to chondrite, as are Sr, Zr, and Rb, with a prominent enrichment in Ba. In comparison to chondrite, CaO, MgO, Mn, Ni, Cr, and Co are depleted (Figure 8a). Normalized trace and major element components against PAAS display a minor enrichment in Ni, Zn, Zr, & Co with a depletion in CaO, Mn, Cr, Cu, and Rb (Figure 8b).

4.4 Provenance and Tectonic Setting

The provenance and tectonic setting of the Zubair oil shale have been defined using elemental ratios and discriminant functions [21] [22] [23] [24]. [25] determined Al_2O_3/ TiO_2 ratios to differentiate mafic Al_2O_3/ TiO_2 14 and felsic Al_2O_3/ TiO_2 from 19 to 28 source rocks, which could be Arabian Shield granodiorite, tonalite, and granites. This ratio (11.81 to 17.87) is high in Zubair shale, indicating a felsic source with few contributors of an intermediate source (Table 2). [26] K_2O/Na_2O ratio is also used as a provenance marker in clastic sedimentary rocks; a reduced value indicates that the source is mafic rather than felsic. The existence of illite and illite-smectite in oil shale samples confirms their origins from an intermediate and felsic source, and K_2O/Na_2O ratios range from 1.11 to 3.71. The zircon content of sediments can also be used to determine their provenance [25]. A binary graph of Zr vs TiO_2 implies that the Zubair oil shale's source rocks are intermediate to felsic igneous rocks sourced from a stable cratonic setting (Figure 7b).

Open Access
No. 40, September 2023, pp. 19-40
P- ISSN: 2220-5381
E- ISSN: 2710-1096

This felsic granitic provenance was also supported by [27] major elemental discriminant illustration, which shows that samples are mostly felsic in origin (Fig. 9a). This felsic provenance is associated with granite, whereas the intermediate provenance is associated with an andesitic mixture or the Arabian Shield's amphibolite, granitic, and magmatic gneisses.

Clastic sediments can be derived from a variety of tectonic settings and have distinct geochemical signatures due to parent rock geochemical composition.

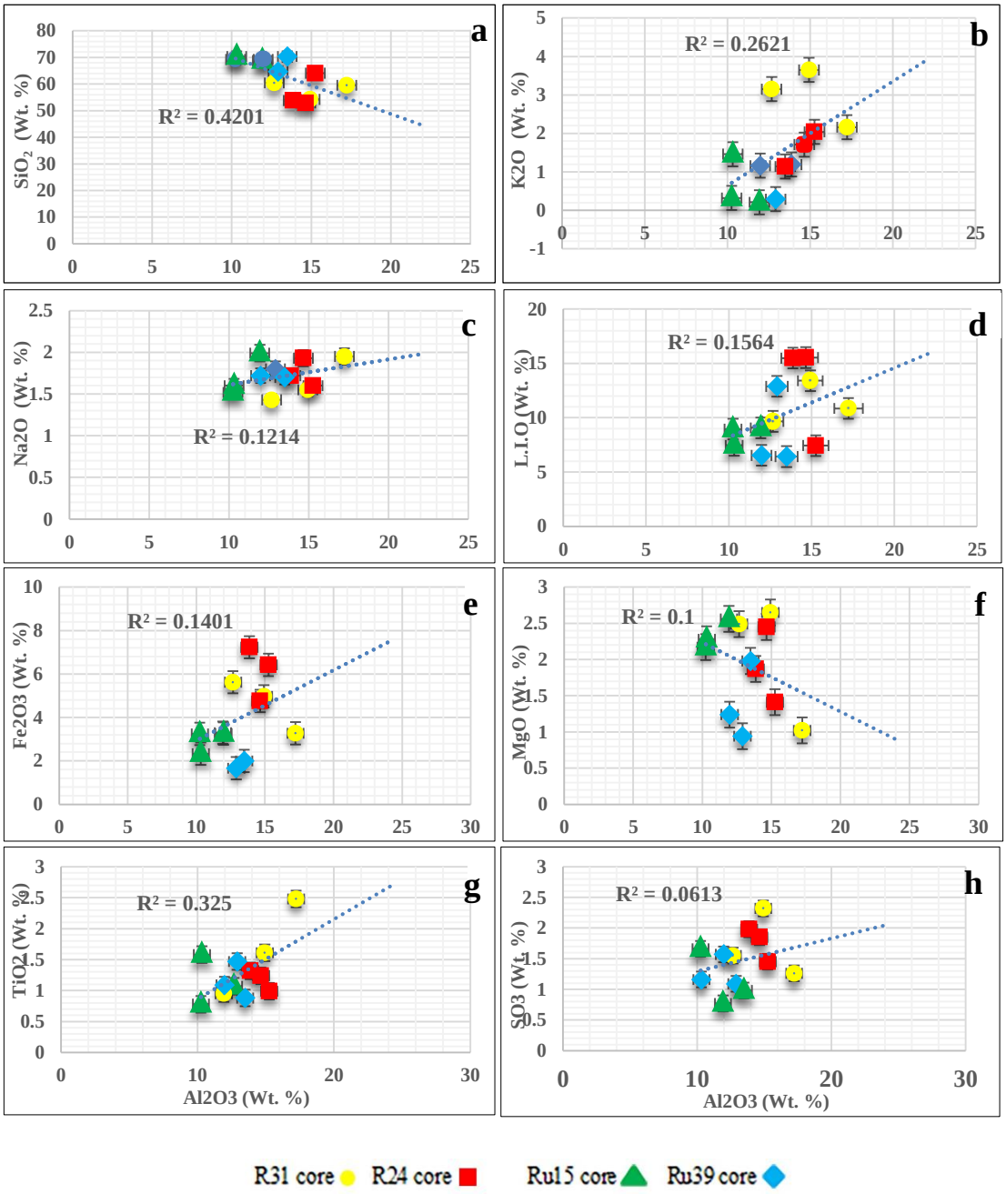

Fig. (6): Al_2O_3 diagram versus selected major oxides.

Open Access
No. 40, September 2023, pp. 19-40

P- ISSN: 2220-5381
E- ISSN: 2710-1096

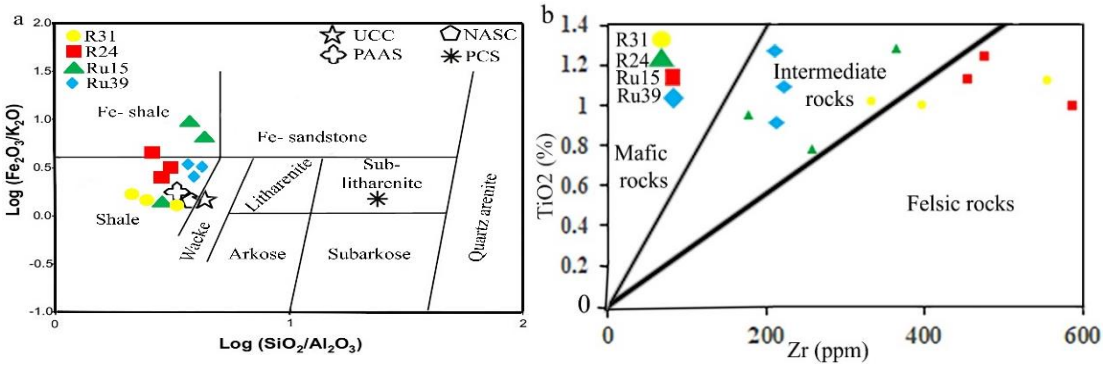

Fig. (7): (a) Geochemical classification of Zubair oil shale focused on the log (SiO_2/ Al_2O_3) vs the log (Fe_2O_3/ K_2O) diagram after [19] and (b) Provenance of major and trace elements, as well as a tectonic diagram based on TiO_2 versus Zr [25].

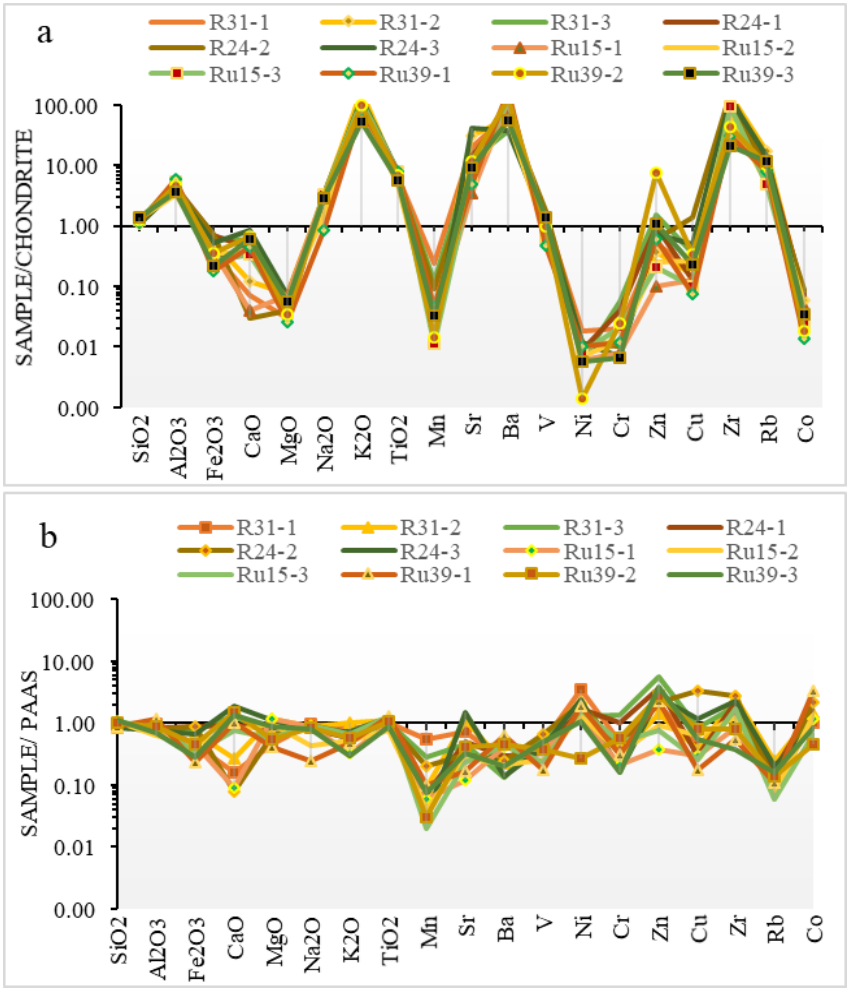

Fig. (8): Normalized multi-element graph for the major element & identified the trace element compositions normalized comparable to (a) chondrite [31] & (b) PAAS [20].

Open Access
No. 40, September 2023, pp. 19-40
P- ISSN: 2220-5381
E- ISSN: 2710-1096

The unique discriminant function graphs rely on the major oxides that have been adjusted to 100% volatile-free [22]. For the low-silica tectonic discrimination [(SiO_2)adj= 52.88- 70.33% (m2)]sediments, discrimination diagrams were proposed [28] [29]. In the collision field, all samples were plotted (Fig. 9b). The unique discriminant diagram (passive & active) suggested relied on the mixture for ten major (SiO2 to L.O.I) and eleven trace elements (Mn to Co) on a volatile-free basis, adjusted to 100% confirm collision setting for Zubair shales. Mostly all samples on this plot are schemed in the passive margin, except one in active margin settings (Fig. 10). In accordance with the geological precursor and geochemical features of the oil shale metamorphic, plutonic, and sedimentary rocks from the Late Berriasian-Albian cycle. The plutonic and metamorphic rocks that drive the Zubair shale formed in collision settings (passive margin) and signified the beginning of the Zubair shale deposit's lower Cretaceous deposit. These hydrocarbons had (in part) charged the Tertiary and Cretaceous reservoirs, particularly the Zubair Formation, formed by Alpine collision traps 15-10 million years ago, which formed folds in the Mesopotamian Basin and closed the Tethys Ocean between the Arabian and Eurasian Plates. This interpretation fits with the geological history of the Zubair oil shale [30].

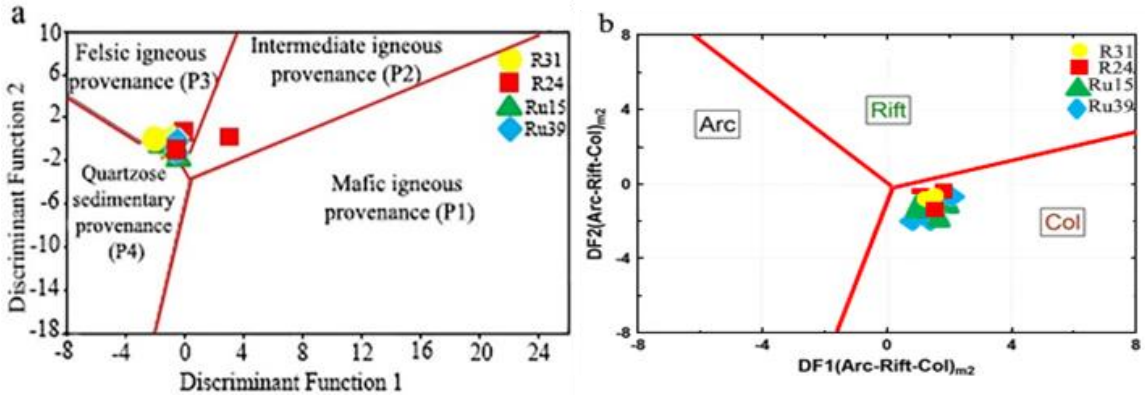

Fig. (9): Major & trace element provenance and tectonic graphs. (a) Discriminant function (F) diagram after [27] where F1 (Discriminant Function 1) = (0.607 × Al_2O_3) + (− 1.773 × TiO_2) + (− 1.5 × MgO) + (0.76×Fe_2O_3) + (0.509 × Na_2O) + (0.616 × CaO) + (K_2O × (− 1.22)) + (− 9.09). F2 (Discriminant Function 2) = (Al_2O_3× 0.07) + (0.445 × TiO_2) + (MgO × (− 1.142)) +(− 0.25 × Fe_2O_3) + (Na_2O ×1.475) + (0.438 × CaO) + (1.426 × K_2O) + (− 6.861); (b) Major elements tectonic setting discrimination diagram [28]. The low-silica diagram is represented by the subscript m2 in DF1 and DF2, where DF1 (Col - Rift -Arc) m2 = (− 1.854 × ln(Al_2O_3/SiO_2)adj) + (0.608 × ln (TiO_2/SiO_2)adj) + (− 0.550 × ln(MnO/SiO_2)adj) + (0.299 × ln(Fe_2O_3t/SiO_2)adj) + (0.194 × ln(CaO/SiO_2)adj) + (0.1120 × ln(MgO/SiO_2)adj) +(1.941×ln(K_2O/SiO_2)adj) + (−1.510 × ln(Na_2O/SiO_2)adj) + (0.003 × ln(P_2O_5/SiO_2)adj) − 0.294. DF2 (Arc-Rift-Col) m2 = (− 0.995 × ln(Al_2O_3/ SiO_2)adj) + (− 0.554 × ln(TiO_2/SiO_2)adj) + (− 1.391 × ln(MnO/SiO_2)adj) + (1.765 × ln(Fe_2O_3t/SiO_2)adj) +(0.225 × ln(CaO/SiO_2)adj) + (− 1.034 × ln(MgO/SiO_2)adj) + (0.330 × ln(K_2O/SiO_2)adj) + (0.713 × ln(Na_2O/SiO_2)adj) + (0.637 × ln(P_2O_5/ SiO_2)adj) − 3.631.

Open Access
No. 40, September 2023, pp. 19-40
P- ISSN: 2220-5381
E- ISSN: 2710-1096

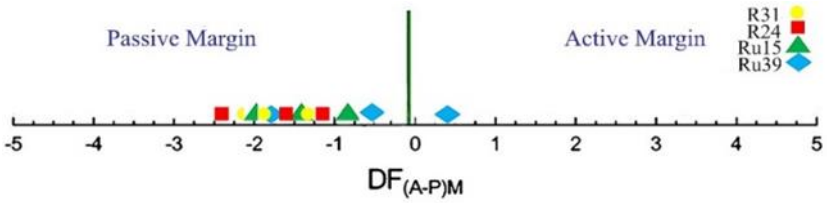

Fig. (10): Diagram of a multidimensional discriminant function discriminating the (A) active and (P)Passive margin settings [29], where DF(A-P)MT = (Ilr1TiO$_2$MT × 3.2683)+ (5.3873 × Ilr2Al$_2$O$_3$MT) + (1.5546 × Ilr3Fe$_2$O$_3$MT) + (3.2166 × Ilr4MnOMT) + (4.7542 × Ilr5MgOMT) + (2.0390 × Ilr6CaOMT)+(4.0490× Ilr7Na$_2$OMT) + (3.1505 × Ilr8K$_2$OMT) + (2.3688 × Ilr9P$_2$O$_5$MT)+(Ilr10CrMT × 2.8354) + (Ilr11NbMT × 0.9011) + (Ilr12NiMT ×1.9128)+(Ilr13VMT × 2.9094) + (Ilr14YMT × 4.1507) + (Ilr15ZrMT × 3.4871)– 3.2088

4.5 Paleo-weathering Conditions and Shale Maturity

Many research's and studies have used various weathering indexes & elemental proportions to assess paleo-weathering mechanisms and also the weathering intensity of source rock [22] [32]. The chemical weathering intensity within the source area is assessed using CIA, PIA, and CIW in this study. The triangular plot A-CN-K (Al_2O_3-CaO* + Na_2O-K_2O) as well specifies a weathering degree and possible source rocks composition [13]. CaO* values have been accepted just when CaO < Na_2O, if CaO > Na_2O, the CaO concentration is assumed to be equivalent to that of Na_2O [17]. The values of CIA for Zubair shale samples range from 70.63 to 86.53% (av.= 78.75%), implying that such source rocks have undergone extensive chemical weathering. High PIA (av. = 87.12%) and CIW (av. = 88.59%) values support this strong chemical weathering (Table 2). The mineralogical analysis also showed a predominance of clay minerals as well as a higher amount of iron oxide coatings, which could be the result of diagenetic alteration or severe weathering inside the area of the source. The existence of kaolinite and illite implies that feldspar and muscovite, which are mineral phases derived from of (granitic) source area, were chemically weathered. As a result, the A-CN-K figure shows that each sample map is high above the feldspar section near kaolinite & illite, chlorite, and gibbsite fields, and follows the A-CN meet the weathering trend towards A-apex (Fig.11a), indicating granites as the primary source rock but as well as reflecting fairly stable conditions of weathering. The difference in value systems for the chemical index in deposits is related to the source rock content. This implication assumes that shales from the Zubair Formation, which were deposited in the collision stage, were probably subjected to tectonic activity. The ICV can be used to determine the maturity of shales [16]. Chemical weathering tends to increase with alumina content and may frequently represent

Open Access
No. 40, September 2023, pp. 19-40
P- ISSN: 2220-5381
E- ISSN: 2710-1096

the maturity of shales. ICV > 1 sediments have abundant unweathered detrital minerals and are compositionally immature, whereas ICV < 1 sediments are composed of weathered minerals (e.g. clay minerals) and are compositionally mature [16]. The ICV values of the examined shales range from 0.33 to 0.99 (av.= 0.70%), implying texturally mature shales deposited inside a tectonically active environment. The ratios of K_2O/Na_2O for such core shales range from 1.11 to 6.2 (av.= 2.68), indicating that the shales are mature. The ratio of SiO_2/Al_2O_3 is frequently used to assess the maturity of the textural of shales, and it ranges from 2.54 to 5.48 (av.=3.91), showed the highest compositional maturity, most likely due to feldspar alteration [13]. The ICV versus CIA binary graph [13] [16] proves the severe weathering and elevated maturity of shales (Fig.11b). As a result, the chemical weathering degree is primarily determined by the source area's climate and erosion. The recycled shale input could represent distal facies deposited in low relief.

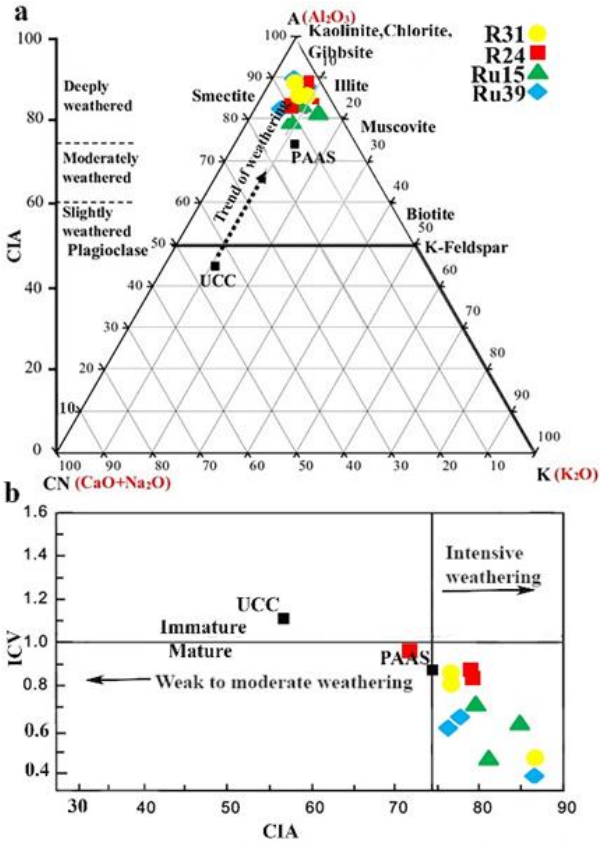

Fig. (11): Diagrams of weathering and maturity for Zubair oil shales. (a) Ternary graph (in mole fraction) of A-CN-K, sample placement specifying severe weathering (chemical). (b) ICV vs CIA chart [13] [16] displaying shales maturity.

Open Access
No. 40, September 2023, pp. 19-40
P- ISSN: 2220-5381
E- ISSN: 2710-1096

4.6 Paleoclimate and Depositional Setting

Weathering index values (CIA and PIA), as well as trace elements (Rb, Sr, and Cu) also their ratios (Sr/Cu and Rb/Sr) are all be regarded a suitable tool for investigating the source area's paleoenvironment. A few research findings have been using Rb/Sr & Sr/Cu ratios to deduce the paleoclimatic conditions that generated the deltaic environment [33] [34]. A humid and warm environment is indicated by low Rb/Sr & Sr/Cu ratios. Clays could indicate climate changes within source areas. Kaolinite is created by severe weathering of feldspars in a subtropical humid climate, while illite is created in a cold climate and very little precipitation. The greater CIA value shows the sediments were deposited in a whole subtropical warm and humid climate. The ratios of Rb/Sr range between 0.11 to 0.59 (ave. 0.21) and the ratios of Sr/Cu range between 0.46 to 3.59 (ave. 2.03), indicating a minimal change throughout the years (Table 3). Climate index C value [where C= $\sum$ (Mn + Fe + Ni + Cr + Co + V / $\sum$ (Mg + Ca + Ba + Sr + Na + K)] has effectively defined paleoclimatic conditions. Sediment C values range from 0.57 to 0.82, implying lesser oscillating paleoclimatic conditions, inferring semi-humid to semi-arid environments (Fig.12a). This suggests that the Zubair oil shale sediments were not subjected to considerable paleoclimatic differences. The elements of Al_2O_3 and V can be used to infer paleoenvironmental conditions in fluvial-deltaic, deltaic, and shallow marine environments. Vanadium concentration in marine facies is relatively better than in freshwater deposits. As clarified by the V-Al_2O_3 plot, sediments have been deposited in fluvial and shallow marine environments, according to binary diagram of paleoenvironmental modeling (Fig.12b). The shallow marine & fluvial depositional environments of shales were oxic and dysoxic, as indicated by Ni/Co ratios ranging from 1.58 to 8.65 (av.=3.30) (Table 3). Moreover, a ratio of Ni/Co for 5 implies an oxic environment, while a ratio of Ni/Co greater than 5 implies an anoxic environment.

Open Access
No. 40, September 2023, pp. 19-40
P- ISSN: 2220-5381
E- ISSN: 2710-1096

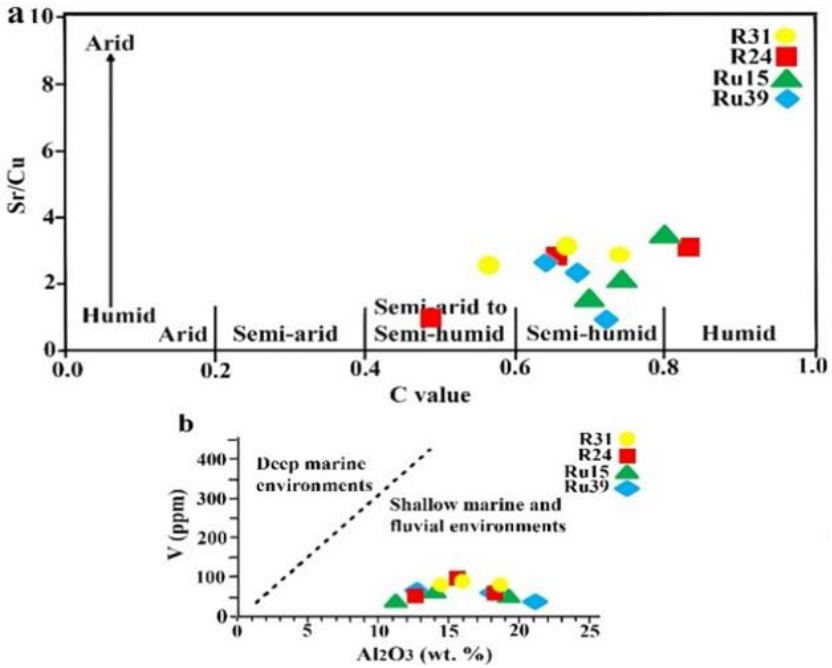

Fig. (12): Binary graph of (a) C value vs Sr/Cu ratio, proposing semi- arid to semi- humid paleoclimatic condition; (b) Al_2O_3 vs V.

5. Conclusions

1- Silty-clayey laminated mudstone lithofacies, mica-rich mudstone lithofacies, clay-rich siliceous mudstone lithofacies, and clay-bearing calcareous mudstone lithofacies were identified through petrographic analysis.

2- Zubair oil shale is a silica-rich argillaceous mudstone type with a high organic matter content. The shales are made up of kaolinite, illite, and smectite, besides quartz, calcite, dolomite, and pyrite.

3- The geochemical composition of Zubair shales demonstrates that they were formed from felsic rocks such as granites to minor quantities of intermediate igneous rocks. Discrimination diagrams indicate passive margin settings (collision) to similar maturity levels.

4- According to the findings of this study, oil shales are strongly weathered and deposition occurs in a warm to the semi-humid environment.

.

Open Access
No. 40, September 2023, pp. 19-40
P- ISSN: 2220-5381
E- ISSN: 2710-1096

References

[1] R. M. Idan, F. A. Al-Musawi, A. L. M. Salih, and S. A. F. Al-Qaraghuli, "The Petroleum System of Zubair Formation in Zubair Subzone, Southern Iraq", Journal of Petroleum Research and Studies, vol. 9, no. 4, pp. 57-73, Dec. 2019. DOI: https://doi.org/10.52716/jprs.v9i4.322

[2] R.M. Idan, R.F. Faisal, M.E. Nasser, T.K. AL-Ameri, and D. AL-Rawi, "Hydrocarbon potential of Zubair Formation in the south of Iraq, "*Arabian Journal of Geosciences*, Vol. 8, no.7, pp. 4805–4817, 2015 b, DOI: https://doi.org/10.1007/s12517-014-1569-6

[3] F.K. Bahman, F.H. Abdullah, A. Saleh and H. Alimi, "Organic geochemical and petrographical characteristics of the major lower cretaceous petroleum source rock (Makhul Formation) in Kuwait, " *Kuwait J. Sci.*, vol.49, no. 1, pp. 1-25, 2022, DOI: https://doi.org/10.48129/kjs.v49i1.10277

[4] S.Z. Jassim and J.C. Goff, "Geology of Iraq, " Dolin, Prague and Moravian Museum, Brno, Czech Republic, p. 341, 2006.

[5] A.K. Abbas, R.E. Flori and M. Alsaba, "Testing and Evaluation of Shale Stability for Zubair Shale Formation, " *Society of Petroleum Engineers*, 192274, pp. 1–9, 2018d, https://doi.org/10.2118/192274-MS

[6] H.K. Almayyahi, M.H. Aljaberi and H. almalikee, " Geochemical Study for the Upper Shale Member – Zubair Formation in Rumaila Oilfield, South Iraq, "*Int. J. of Mining Science*, vol. 4, no. 4, pp. 56-75, 2018, DOI: http://dx.doi.org/10.20431/2454-9460.0404006

[7] A.F. Nader, R.J. Muhammad, W.M. Saleh, M.S. Abdullah and A.Q. Atwan, "Evaluation of main pay- Zubair Formation after operations re-injection of produced water directly in Rumaila Oil Field norths under matrix condition, " *J. of Petroleum Research & Studies*, no.35, pp.13- 26, 2022, DOI: https://doi.org/10.52716/jprs.v12i2.655

[8] M.K. Al-Jafar and M.H. Al-Jaberi, "Determination of clay minerals using gamma ray spectroscopy for the Zubair Formation in Southern Iraq. *Journal of Petroleum Exploration and Production Technology*, " 2021. https://doi.org/10.1007/s13202-021-01371-3

[9] W. Bleam, "Soil and Environmental Chemistry, " Elsevier, Amsterdam, 2nd Edition, 573p., 2017.

[10] H.G. Dill, "Kaolin: Soil, rock and ore: From the mineral to the magmatic, sedimentary and metamorphic environments, "*Earth- Science Reviews*, vol. 161, pp. 16-129, 2016, https://doi.org/10.1016/j.earscirev.2016.07.003

Open Access
No. 40, September 2023, pp. 19-40
P- ISSN: 2220-5381
E- ISSN: 2710-1096

[11] F. Bergaya, B.K.G. Theng and G. Lagaly, "Handbook of Clay Science, " Elsevier, 1st Edition, 1224p., 2006.

[12] K.S. Glaser, C.K. Miller, G.M. Johnson, R.L. Kleinberg and W.D. Pennington, "Seeking the sweet Spot: Reservoir and completion quality in organic shales, " *Oilfield Rev*., vol. 25, pp. 16–29, 2014.

[13] H.W. Nesbitt and G.M. Young, "Prediction of some weathering trends of plutonic and volcanic rocks based on thermodynamic and kinetic considerations, "*Geochimica et Cosmochimica Acta*, vol. 48, pp.1523–1534, 1984, https://doi.org/10.1016/0016-7037(84)90408-3

[14] C.M. Fedo, H. Nesbitt and G.M. Young, "Unraveling the effects of potassium metasomatism in sedimentary rocks and paleosols, with implications for paleoweathering conditions and provenance, " *Geol*., vol. 23, pp. 921–924, 1995, https://doi.org/10.1130/0091-7613(1995)023<0921:UTEOPM>2.3.CO;2

[15] L. Harnois, "The CIW index: a new chemical index of weathering, " *Sediment. Geol.*, vol. 55, pp.319–322, 1988, https://doi.org/10.1016/0037-0738(88)90137-6

[16] R. Cox, D.R. Lowe and R.L. Cullers, "The influence of sediment recycling and basement composition on evolution of mudrock chemistry in the southwestern United States, " *Geochim Cosmochim Acta*, vol.59, pp. 2919–2940, 1995, DOI: 10.1016/0016-7037(95)00185-9

[17] S.M. McLennan, S.R. Taylor, M.T. McCulloch and J.B. Maynard, "Geochemical and Nd/Sr isotopic composition of deep-sea turbidites: crustal evolution and plate tectonic associations, " *Geochim Cosmochim Acta*, vol. 54, pp. 2015–2050, 1990, DOI**:**10.1016/0016-7037(90)90269-Q

[18] K. Yan, C.L. Wang, S. Mischke and J.Y. Wang, "Major and trace-element geochemistry of Late Cretaceous clastic rocks in the Jitai Basin, southeast China, " *Scientific Reports*, vol.11,13846, 2021, Doi: https://doi.org/10.1038/s41598-021-93125-8.

[19] M.M. Herron, "Geochemical classification of terrigenous sands and shales from core and log data," *Journal of Sedimentary Petrology*, vol. 58, pp. 820–829, 1988, https://doi.org/10.1306/212F8E77-2B24-11D7-8648000102C1865D

Open Access
No. 40, September 2023, pp. 19-40
P- ISSN: 2220-5381
E- ISSN: 2710-1096

[20] S.R. Taylor and S.M. McLennan, "The continental crust: its composition and evolution, " Oxford: Blackwell, 312 p, 1985, https://doi.org/10.1002/gj.3350210116

[21] G. Ngueutchoua, A.Z.E. Bessa, J.T. Eyong and D.D. Zandjio, "Geochemistry of cretaceous fine-grained siliciclastic rocks, Douala sub-basin, SW Cameroon: implications for weathering intensity, provenance, paleoclimate, redox condition, and tectonic setting, " *J. Afr. Earth Sci.*, vol.152, pp. 215–236, 2019, https://doi.org/10.1016/j.jafrearsci.2019.02.021

[22] A.Z. Ekoa Bessa, P.D. Ndjigui, G.C. Fuh and J.S. Armstrong-Altrin, "Mineralogy and geochemistry of the Ossa lake Complex sediments, Southern Cameroon: implications for paleoweathering and provenance, " *Arab. J. Geosci.*, vol. 14, 322, 2021, DOI: 10.1007/s12517-021-06591-9

[23] M.A. Farooqui, K.U. Rehman and A. Yaseen, "Petrography, geochemistry and depositional model of Ispikan Conglomerate, Southwest Pakistan, " *Kuwait J. Sci.*, vol. 49, no.1, pp. 1-25, 2022, https://doi.org/10.48129/kjs.v49i1.10486

[24] T. Boschetti, S.M. Awadh, H.S. Al-Mimar, P. Iacumin, L. Toscani, E. Selmo, Z.M. Yaseen, "Chemical and isotope composition of the oilfield brines from Mishrif Formation (southern Iraq): Diagenesis and geothermometry," *Marine and Petroleum Geology*, 1;122: 104637, 2020, https://doi.org/10.1016/j.marpetgeo.2020.104637

[25] K.I. Hayashi, H. Fujisawa, H.D. Holland and H. Ohmoto, "Geochemistry of~ 1.9 Ga sedimentary rocks from northeastern Labrador, Canada, "*Geochim Cosmochim Acta*, vol. 61, pp. 4115–4137, 1997, https://doi.org/10.1016/S0016-7037(97)00214-7

[26] P.E. Potter, "Petrology and chemistry of modern big river sands, " *J. Geol.*, vol. 86, pp. 423–449, 1978, https://doi.org/10.1086/649711

[27] B.P. Roser and R.J. Korsch, "Determination of tectonic setting of sandstone-mudstone suites using SiO_2 content and K_2O/Na_2O ratio, " *J. Geol.*, vol. 94, pp. 635–650, 1986, https://doi.org/10.1086/629071

[28] S.P. Verma and J.S. Armstrong-Altrin, "New multi-dimensional diagrams for tectonic discrimination of siliciclastic sediments and their application to Precambrian basins, " *Chem. Geol.*, vol. 355, pp.117–133, 2013, https://doi.org/10.1016/j.chemgeo.2013.07.014

[29] S.P. Verma and J.S. Armstrong-Altrin, "Geochemical discrimination of siliciclastic sediments from active and passive margin settings, " *Sediment. Geol.*, vol. 332, pp.1–12, 2016, https://doi.org/10.1016/j.sedgeo.2015.11.011

Open Access
No. 40, September 2023, pp. 19-40
P- ISSN: 2220-5381
E- ISSN: 2710-1096

[30] M.F. Al-Shahwan and F.M. Al-Najm, "Tectonic evolution of southern part of the Mesopotamian foredeep basin, " *J. of Petroleum Research & Studies*, vol.30, no.3, pp.1- 17, 2021, https://doi.org/10.52716/jprs.v11i1.425

[31] W.F. McDonough and S.S. Sun, "The composition of the earth, " *Chem. Geol*., vol.120, pp. 223–253, 1995, https://doi.org/10.1016/0009-2541(94)00140-4

[32] A.Z. Ekoa Bessa, G. Ngueutchoua and P.D. Ndjigui, "Mineralogy and geochemistry of sediments from Simbock Lake, Yaoundé area (southern Cameroon): provenance and environmental implications, " *Arab J. Geosci*, vol.11, 710, 2018, DOI: 10.1007/s12517-018-4061-x

[33] J.S. Armstrong-Altrin, Y.I. Lee and J.J. Kasper-Zubillaga, "Mineralogy and geochemistry of sands along the Manzanillo and El Carrizal beach areas southern Mexico: implications for palaeoweathering, provenance and tectonic setting, " *Geol. J.*, vol. 52, pp. 559–582, 2017, https://doi.org/10.1002/gj.2792

[34] J.S. Armstrong-Altrin, A.V. Botello and S.F. Villanueva, "Geochemistry of surface sediments from the northwestern Gulf of Mexico: implications for provenance and heavy metal contamination, "*Geol. Q*, vol. 63, pp. 522–538, 2019, DOI: http://dx.doi.org/10.7306/gq.1484